Analyst

PAPER

View Article Online
View Journal | View Issue

Cite this: *Analyst*, 2016, **141**, 2515

Rapid prototyping of electrochemical lateral flow devices: stencilled electrodes†

Miguel Aller Pellitero,[a] Maria Kitsara,[a] Friedrich Eibensteiner[b] and F. Javier del Campo*[a]

A straightforward and very cost effective method is proposed to prototype electrodes using pressure sensitive adhesives (PSA) and a simple cutting technique. Two cutting methods, namely blade cutting and CO_2 laser ablation, are compared and their respective merits are discussed. The proposed method consists of turning the protective liner on the adhesive into a stencil to apply screen-printing pastes. After the electrodes have been printed, the liner is removed and the PSA can be used as a backing material for standard lateral flow membranes. We present the fabrication of band electrodes down to 250 μm wide, and their characterization using microscopy techniques and cyclic voltammetry. The prototyping approach presented here facilitates the development of new electrochemical devices even if very limited fabrication resources are available. Here we demonstrate the fabrication of a simple lateral-flow device capable of determining glucose in blood. The prototyping approach presented here is highly suitable for the development of novel electroanalytical tools.

Received 24th November 2015,
Accepted 7th March 2016

DOI: 10.1039/c5an02424b

www.rsc.org/analyst

Introduction

The principles of screen-printing, which consists in the deposition of a paste or ink through a lithographically patterned mesh, are well established.[1,2] The microelectronics revolution and the wide availability of conducting and dielectric pastes enabled screen-printing, a set of techniques originally developed by the graphic arts industry, to consolidate the field known as thick-film technologies in the 1960s. Electrochemists have also known screen-printing for decades, and the first fully printed electrochemical devices appeared in the early 1980s in the form of solar cells.[3] Later, screen-printed electrodes began to be used more widely by the electroanalytical community after the success of the first commercial glucose biosensors, nearing the 1990s.[4] Today, screen-printed electrodes constitute very familiar and often essential tools in the electroanalytical research laboratory, as discussed in recent reviews.[5,6]

The advantages that make screen-printing ideal for mass production purposes are its high processing speeds and reproducibility, the possibility to print virtually any material imaginable, and the resulting low unit cost of the produced devices. Printing electrodes involves the confinement of an electrode material layer to a defined shape by a suitable dielectric layer. However, in spite of this apparently simple construction and the versatility of screen-printing techniques, which enables the printing of any desired electrode material into lines a few tens of microns wide[7] and down to 3–5 microns thick, most screen-printed electrodes currently in use are commercial macroelectrodes 1–4 mm in size.[5,6] So while the commoditization of screen printing electrodes has enabled the development of a multitude of new electroanalytical methods using disposable and low-cost substrates, the need for screens in the process can compromise the suitability of the technique for prototyping purposes. This is because most users do not have access to a screen-printer, and even those who have it normally lack the ability and resources to make screens by themselves. Outsourcing the screens results in additional costs and delays in the workflow, which may go against the notion of "rapid" prototyping. The ideal alternatives to this are digital techniques such as ink-jet printing, which allow the "direct" printing of structures without the need for stencils or other ancillaries.[8] Another important difference to screen-printing is that ink-jet printing enables the simultaneous deposition of several materials in the same printing step. Because of this, ink-jet printing is starting to be adopted, mostly for the development of printed electronic devices,[9] but also in the development of electrodes for electrochemical applications, including glucose biosensors.[10,11] However, the adoption of ink-jet printing in research environments is still comparatively expensive because of the capital cost of the equipment, but also due to the limitations associated with the inks and the printing

[a]*Institut de Microelectrònica de Barcelona, IMB-CNM (CSIC). 08193, Bellaterra, Barcelona, Spain. E-mail: Javier.delcampo@csic.es; Tel: +34 935947700*
[b]*Prelonic Technologies. Technisches Buero fuer Technische Chemie, Lannergasse 7, 4020 Linz, Austria. E-mail: f.eibensteiner@prelonic.com; Tel: +43 6647686246*
†Electronic supplementary information (ESI) available. See DOI: 10.1039/c5an02424b

process itself. There are still few commercial inks suitable for electrochemical applications.

These inks are usually costly, they have a short shelf-life, and some (particularly those containing metal particles) require high sintering temperatures that not all substrates can withstand. In addition, users of the technique need to be highly trained. So despite the theoretical suitability of ink-jet techniques for the "rapid" fabrication of highly customized electrodes and circuitry, its present high cost makes this technique inaccessible for most laboratories.

Thus, we seem to be caught at a crossroads between the possibly prohibitive costs of ink-jet printing and the seeming tediousness of screen-printing. This work presents a simple technique that benefits from the wide availability of affordable screen-printing pastes, and the versatility of xurography[12] or, alternatively, laser cutting[13] to stencil electrodes directly onto laminated, pressure-sensitive adhesive materials.[14–16] These substrate materials are typically used as backing tapes in the construction of lateral flow devices, and in this work we show how to use their protective liner as a stencil to make rapid electrode prototypes using either commercial or customized screen printing pastes.

To the best of the authors' knowledge, very few works have addressed the (rapid) prototyping of electrodes for the development of novel electroanalytical flow devices. Godino *et al.* described a methodology to make channel flow cells using a combination of wax printing and stencil lithography.[17] We believe that the methodology presented here represents a more accessible alternative to the prototyping of electrochemical flow devices than the approach described by Godino *et al.*, as it simplifies the work-flow and requires only affordable equipment. Due to the increasing interest in so-called paper microfluidics,[18,19] and the development of cost-effective devices for resource limited settings,[20–24] here we present a simple lateral flow set-up that facilitates the development of electrochemical sensors based on screen-printing pastes. A glucose biosensor is used to highlight the advantages of working with such a set-up, such as the absence of pumps, the ability to work with small samples with next to no dead-volume, and above all offering a high degree of customization at very low cost.

Experimental

Chemicals and materials

The chips presented here were designed using VectorWorks 2015, Student Edition (Techlimits, ES). A CAMM1-GX24 Servo cutter plotter (Roland DG Ibérica, ES) and a 30 W Epilog Mini-24 CO_2 laser engraver (Laser Project, ES) were used to cut pieces of both ARcare® 8259 (Adhesives Research Ltd, IE) pressure sensitive adhesive, and Whatman Fusion 5 (GE Healthcare, FR) lateral flow membranes. The laser system was also used to make a PMMA custom alignment tool to assemble the devices with better than 100 μm tolerance. Ag/AgCl (ref. C61003P7) and carbon (C2030519P4) screen printing pastes from Gwent Electronic Materials Ltd, UK, were used to make the electrodes. 1-Ethoxy-2-propanol, 95%, (ACROS Organics, ES) was used to clean the squeegee used to print the electrodes.

Optical microscopy images were obtained using a Leica DM-4000 microscope. Information on electrode thickness and surface roughness (determined using the root mean square roughness parameter, RMS) was obtained by confocal microscopy measurements on a PLμ 2300 non-contact confocal imaging profiler system attached to a Nikon microscope using a 10× magnification lens. The system was controlled using PLμ proprietary software (Sensofar, Spain). Scanning electron microscopy (SEM) images of the different electrodes were recorded in an Auriga (Carl Zeiss) system. The measurements were performed by applying a beam voltage of 1 kV. Images at different magnifications were obtained on at least three different areas in the same sample using the SE2 detector. Water contact angle measurements were performed using the EasyDrop Standard system (Krüss). The circle method was used for the determination of the sessile drop contact angles. The measurements took place at room temperature (20 °C) and the volume of the applied drops of deionized water was 1.5 μl. Contact angle data were obtained by averaging over five measurements in different areas on the sample surface.

Electrochemical measurements were carried out using a μ-Autolab III potentiostat (Metrohm) controlled by a PC running GPES 4.1 software. A solution of 50 mM phosphate buffer (Fluka) and 0.1 M KCl (Sigma-Aldrich) at pH = 7 was used as the supporting electrolyte. Voltammetric measurements were done in a 5 mM potassium hexacyanoferrate(II) trihydrate (Sigma-Aldrich) solution. Amperometric measurements were done in glucose (Sigma-Aldrich) solutions prepared in the supporting electrolyte. Electrodes were activated with potential steps in 0.5 M KNO_3 (Sigma-Aldrich) to improve the electrode kinetics.[25,26]

Glucose oxidase, GOx, (Sekisui Diagnostics, EC 1.1.3.4, 236 U mg^{-1}), glutaraldehyde (Sigma-Aldrich, 50% w/w), bovine serum albumin, BSA (Sigma-Aldrich), alcoholic Nafion solution, 20% w/w (Sigma-Aldrich), and *N*,*N*,*N*′,*N*′-tetramethyl-*p*-phenylenediamine, TMPD (Sigma-Aldrich) were used for the construction of the glucose biosensor. All chemicals were of analytical grade and were used as received.

Electrode fabrication

Fig. 1 describes the approach demonstrated in this work, which consists of the fabrication of stencils *in situ* on pressure sensitive adhesive films by a simple cutting operation. These stencils can be used to print electrodes using any screen-printing paste, in three steps: (i) cutting the pressure sensitive adhesive sheets and lateral flow membranes, (ii) depositing and curing the electrode pastes, and (iii) device assembly.

Pressure sensitive adhesive sheets and lateral flow membranes could both be cut using the cutter plotter or the laser engraver. The technique is easier to implement with the cutter plotter, but laser cutting affords much faster processing speeds and, in the case of lateral flow membranes, laser cutting leads to better results because it is a contact-less cutting technique. Although it is in principle possible to cut these membranes

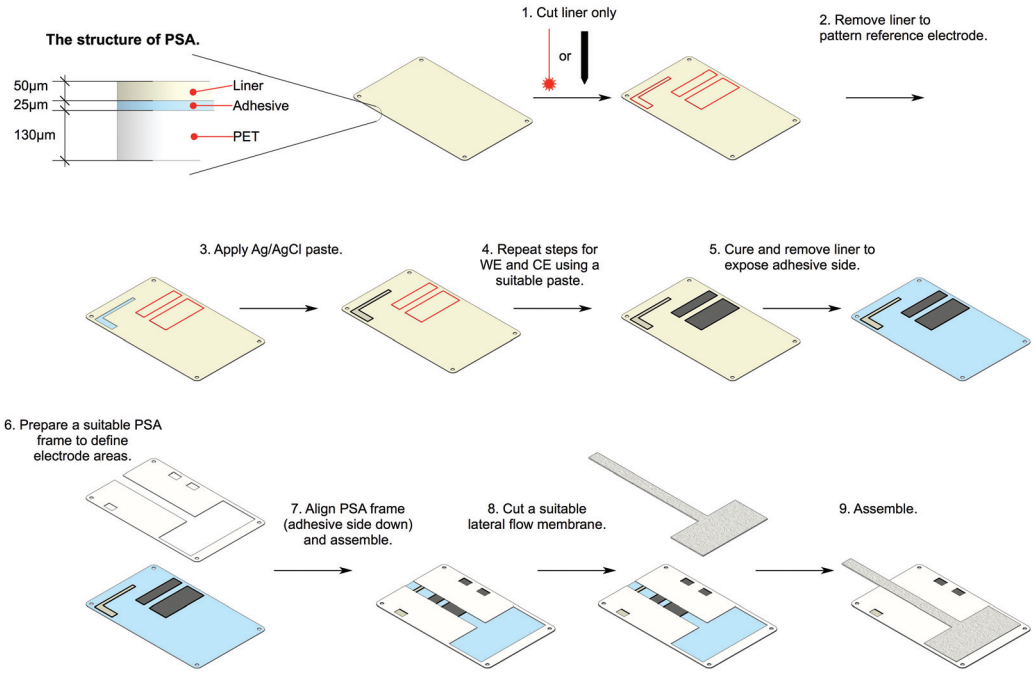

Fig. 1 Diagrammatic representation showing the rapid fabrication of electrodes for electrochemical detection in lateral flow devices. The liner of a pressure sensitive adhesive sheet is pre-cut and selectively removed, which transforms it into a stencil. Laser or blade cutting can be used interchangeably.

using a cutter plotter, the blade can easily tear off the material, leading to significantly lower fabrication yields.

The stencils were made by cutting through the 50 μm-thick siliconized polyester liner protecting the adhesive layer of the pressure sensitive adhesive. Three electrodes were pre-cut in the liner. Although smaller dimensions can be achieved, the widths of these electrodes were 1, 3 and 5 mm for the pseudo-reference, working, and auxiliary electrodes, respectively. First, the pseudo-reference electrode was printed with a single layer of the Ag/AgCl paste. Next, the liner was removed from the working and auxiliary electrode areas, and a graphite paste was applied. To overcome the appearance of cracks in these electrodes, and to improve electrode performance, up to three paste layers could be applied followed by corresponding curing steps.

In order to define the active electrode areas and contacts, a second PSA layer was cut. This second layer was stacked on the electrode substrate with its adhesive side face down. This is important to seal the electrodes in the device and thus prevent the solution from creeping by capillary action through the gap between the printed electrode and its cover, which would lead to leak currents and electrochemical noise. Once the electrodes are adequately sealed, a lateral flow membrane can be fitted into the socket left by the PSA cover, as shown in Fig. 1.

Glucose biosensor construction

Glucose biosensors were constructed on 3 × 3 mm carbon electrodes as follows: 10 μL of a 25 mM TMPD solution prepared in ethanol (96%) were spread on the surface of the working electrode and allowed to dry at room temperature. Next, 50 μL of a solution containing 30 mg mL^{-1} GOx, 0.3% (w/w) glutaraldehyde, and 1.2 mg mL^{-1} BSA prepared in the supporting electrolyte was mixed with 50 μL of an alcoholic 1% (w/w) Nafion solution and vigorously stirred. 5 μL of this solution was cast on the TMPD film and dried overnight at 4 °C in darkness. The electrode was thoroughly rinsed with deionised water, and then polarized at 0.2 V *vs.* Ag/AgCl for 10 minutes in the supporting electrolyte until a low, stable background current was observed. The electrode was then ready to use. The experiments were performed in compliance with CSIC's guidelines for experimentation with animal and/or human subjects, and the experiments were approved by CSIC's bioethics committee within the framework of the DADDI2 project.

Results and discussion

We set out to find the critical dimensions of this technique; that is, the size of the smallest features that can be stencilled with confidence. Electrodes with nominal sizes ranging from 3 mm to 250 μm were fabricated using both laser engraving and xurography, and compared. Although it was possible to make electrodes with nominal dimensions less than 250 μm, their yield was too low to be considered of interest, and therefore we concluded that the practical limit for both techniques was the fabrication of 250 μm structures. This is in agreement with other works reporting on the fabrication of structures using xurography[27] and CO_2 laser ablation.[28] Note that the current state of the art in screen-printing enables the production of lines down to *ca.* 30 μm using very high-quality

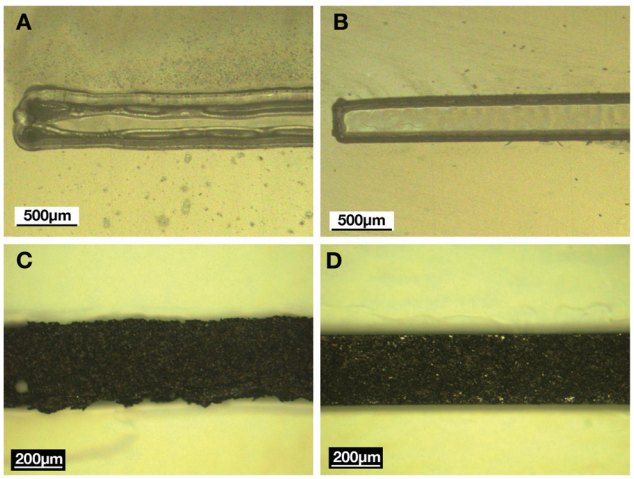

Fig. 2 Optical microscopy images of stencils fabricated with laser (A) or cutter plotter (B), and carbon working electrodes printed using stencils cut with laser (C) or cutter plotter (D).

(and costly) stainless steel mesh screens.[20] However, given the low level of resources involved, the method proposed here is very adequate for prototyping purposes.

We would like to stress the important role of the stencils on the final quality of the electrodes produced. The technique employed to cut the liner on the PSA affects the way that the working carbon electrodes are printed and, consequently, their electrochemical response. Fig. 2 shows images of both stencils and printed bands of 250 μm nominal width, cut by both methods. The figure shows that a cleaner cut is achieved with the cutter plotter (right-hand side images), which results in electrodes printed with a sharper definition.

The difference in the quality stems from the nature of the cutting operation itself. Blade cutting is a contact technique that relies on the selection of a suitable blade and the optimization of blade force and cutting speed.[12] Blade cutting yields well-defined, homogeneous and continuous cut lines. Laser cutting, on the other hand, is a non-contact technique that removes material by ablation, using pulsated light of sufficient energy. The results obtained by laser cutting depend on a number of factors,[13] so that cut depth needs to be adjusted by trial and error through the optimization of key parameters such as laser power, pulsation frequency, and raster speed. On close inspection, the cut-line seems discontinuous and it is often possible to observe the points where the laser beam pulses melted the substrate. Table 1 shows that blade cutting led to slightly better results than laser cutting. The fabrication accuracy data, reported in the leftmost column for each technique, refer to the difference between the nominal and actual size of the fabricated structures. The table shows that fabrication accuracy is comparable using either of the two methods, however the size of cutter-plotter cut stencils is highly affected by working conditions such as the cutting force and the quality of the blade, which can bring about differences in batch-to-batch reproducibility for the smaller structures. The reason for this is found in the width of the cut-line achieved by each technique. The laser has a spot size of around 125 microns while the cutter plotter presents a cut width of around 50–75 microns for brand-new blades. However, greater cut-line widths may be obtained if excessive cutting force and/or blunted blades are used. Having said this, it is possible to make structures of a desired size simply by taking the cut-line width into consideration at the design stage. These considerations may not be so important in the fabrication of large structures, but they need to be paid attention to if smaller features need to be made, or if a higher accuracy and quality are desired. In fact, corrections of this kind were made in the definition of the device alignment marks. The second column in Table 1 reports on the repeatability of the technique, defined as the RSD of projected area measurements corresponding to a fabrication batch of 32 chips (8 for each working electrode size). Here both techniques display a high repeatability, although the cutter-plotter technique leads to slightly better results when dealing with small features. The third column in Table 1, on current response repeatability, reports the deviations found in the peak current for each set of devices.

Differences in thickness between different electrodes can be expected because the electrodes are made manually. Typically we found that different electrodes could present thicknesses between 50 and 85 μm. In the smallest bands, which are 250–300 μm wide, the area of the side faces is comparable in magnitude to that of the top face for the smallest electrodes produced, and they may account for over 40% of the current recorded. The contribution of the electrode sides becomes less than 10% for 3 × 3 mm electrodes made by either technique. However, current response repeatability correlates with fabrication repeatability, suggesting that differences in electrode thickness are very small for this particular batch. Last, in addition to the differences in electrode quality obtained through the two methods discussed, we would also like to outline some of the differences existing

Table 1 Comparison of devices fabricated with the two techniques (n = 8)

	Laser cut devices			Blade cut devices		
Nominal width (mm)	Fabrication accuracy (%)	Fabrication repeatability (%RSD)	Current response repeatability (%RSD)	Fabrication accuracy (%)	Fabrication repeatibility (%RSD)	Current response repeatability (%RSD)
0.25	28	8	7	34	2	5
0.50	11	3	6	11	2	4
1.00	12	3	6	9	3	5
3.00	2	1	4	3	1	3

between both techniques in terms of cost structure and processing speeds. Setting up a laser engraving system requires a significantly larger capital investment than a plotter cutter.

However, the cost of the blades used by the plotter, together with its slower processing speeds, may result in higher running costs compared to a laser system. We believe that, due to its much faster processing speeds, the laser is ideal for the production and testing of several designs in a short time. On the other hand, a plotter can be an ideal solution for the production of high-quality and yet cost effective prototypes in the laboratory, and for laboratories with more limited resources.

Electrode characterization

We studied the effects of curing conditions (time and temperature) and the number of material layers deposited on the physical and electrochemical properties of the electrodes.

According to the manufacturer, the pastes used in the fabrication of the electrodes presented here can be cured at temperatures as low as 60 °C. However, to facilitate the removal of volatile compounds present in the pastes, the electrodes were cured at 90 °C. The curing time was also optimized, finding that 15 minutes at 80–90 °C sufficed to dry the pastes completely after each printing step. Fig. 3 shows a series of devices with band electrodes of widths ranging from 250 μm to 3 mm. We analyzed the dependence of both peak current, I_p, and peak-to-peak separation, ΔE_p, with scan-rate, ν, in the range from 5 mV s^{-1}–2 V s^{-1}. Fig. 4 shows the representation of I_p *vs.* $\nu^{1/2}$ for a typical electrode. The data presents a linear region consistent with a planar diffusion controlled system up to *ca.* 200 mV s^{-1}. The current deviates significantly at higher scan rates, indicating sluggish electron transfer kinetics. We measured the electron transfer rate constant from the ΔE_p – Log(ν) dependence using the methods of Matsuda–Ayabe,[30] and the more recent by Lavagnini *et al.*[29] Both methods led to comparable results, although the one by Lavagnini *et al.* has two important limitations. First, it is restricted to cases where $\Delta E_p \leq 200$ mV and, second, since it averages data from low scan rates it may lead to an overestimated k_s value. The method by Matsuda and Ayabe, on the other hand, may give a better estimation of the true k_s, as it uses the faster scan rates to determine the point of departure from ideality (see Fig. 1S, ESI†). Thus, according to Lavagnini's method, $k_s = 8.62 \times 10^{-3}$ cm s^{-1}, whereas following that by Matsuda and Ayabe leads to $k_s = 5.04 \times 10^{-3}$ cm s^{-1}. However, if Lavagnini's method is applied to the data recorded at 100 mV s^{-1}, according to Matsuda and Ayabe's method for $\Lambda = 1$ and $\Delta E_p = 125$ mV then we obtain $k_s = 5.2 \times 10^{-3}$ cm s^{-1}. Here $\Lambda = k_s/\sqrt{(nFD\nu/(RT))}$; in this case we used a diffusion coefficient value of 6.5×10^{-10} m^2 s^{-1} for ferrocyanide. R is the gas constant, T is the absolute temperature and ν is the scan rate in V s^{-1}. In summary, despite their quasi-reversible kinetics these electrodes may be used in amperometry.

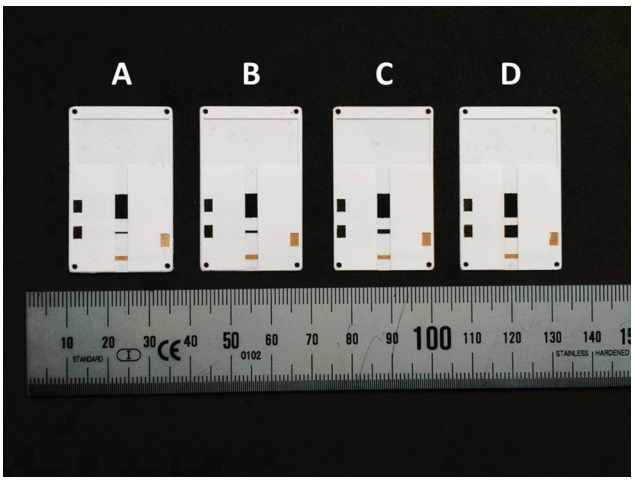

Fig. 3 Four chips featuring carbon band electrodes of 250 μm (A), 500 μm (B), 1 mm (C), and 3 mm (D) widths.

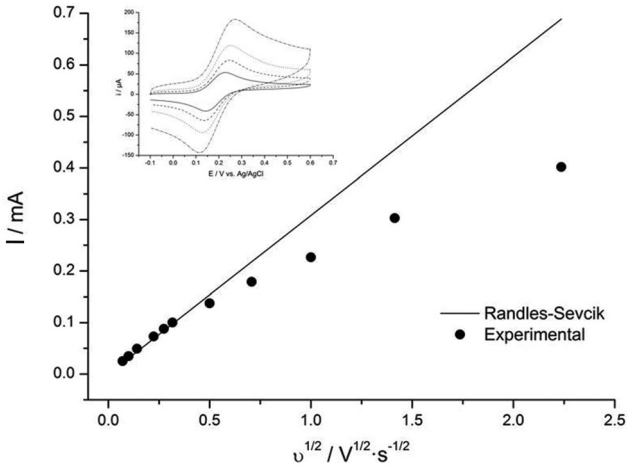

Fig. 4 Peak current as a function of the square root of the scan rate for cyclic voltammograms obtained in 5 mM ferrocyanide in supporting electrolyte, and the Randles–Sevcik equation prediction for a 3 mm chip. The inset shows the voltammograms at different scan rates (20, 50, 100 and 250 mV s^{-1}).

Fig. 4 and 5 show typical results of the electrochemical and physical characterization measurements, respectively, carried out on electrodes made by the application of three carbon paste layers. Electrodes made from one, two, and three layers of the carbon paste were compared.

Table 2 summarizes the physical and electrochemical properties displayed by these electrodes. Voltammetric measurements were carried out in 5 mM ferrocyanide solutions with a selected scan rate of 20 mV s^{-1}. The data show that the oxidation and reduction peak-to-peak separation decreases and the electron transfer rate constant improves as the number of layers increases from one to three. From the peak-to-peak separations observed, we estimated the electron transfer rate constant to be between 6×10^{-4} cm s^{-1} and 4×10^{-3} cm s^{-1}, for electrodes made of one or three carbon paste layers, respectively.[29] This improvement in the electrochemical response when more carbon paste is applied is also likely related to a decrease in electrode resistance. As the data show, the electrical resistance of the carbon electrodes, measured along a 5 × 3 mm track, decreases with increasing thickness.

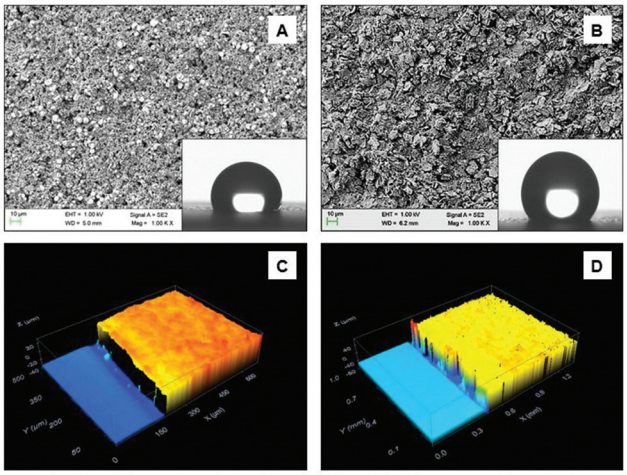

Fig. 5 SEM images of Ag/AgCl (A) and carbon electrodes (B) and their respective 3-D profiles obtained by confocal microscopy, (C) and (D). The insets of (A) and (B) contain water contact angle images of the fabricated electrodes.

A high electrical resistance typically results in distorted cyclic voltammograms displaying an upward baseline and increased peak-to-peak separations. However, the resistance of the electrodes produced here is not sufficient to produce these effects, and all the voltammograms recorded rest on a flat baseline (see Fig. 2S, ESI†).

Screen-printed electrodes display electrochemically heterogeneous surfaces;[31,32] in the present case, graphite particles are embedded in an inert polymer matrix. On the other hand, the solvent in the ink can also dissolve the adhesive on which the paste is applied. Thus, we believe that on the first application of paste, the latter mixes with the adhesive and this results in the sluggish electron transfer observed in electrodes made with a single carbon paste coating. As more carbon paste is applied, the relative amount of graphite present increases, and the electrochemical properties improve. Although surface roughness can also affect electrochemical behaviour, in this case roughness did not seem to be a determining factor, as suggested by our RMS data.

Last, although contact angle measurements are not conclusive, electrodes with more carbon coatings seem to be slightly less hydrophobic. Since surface roughness is the same, this difference in contact angle is again thought to be due to changes in electrode composition. Moreover, we also wanted to rule out the possibility that the changes in electrode composition were due to the curing conditions. It has been reported that increasing the curing temperature brings about a decrease in contact angle between water and the carbon electrode surface.[33] Because electrodes consisting of three carbon paste coats were annealed for a total of 45 minutes, we also cured electrodes consisting of a single coating for up to 45 minutes, and studied their electrochemical response. Cyclic voltammetry data from these electrodes shows that their electrochemical performance is significantly worse than that of electrodes made from three carbon paste coatings (see Fig. 3S, ESI†). So, although the contamination mechanism is not fully understood, it is clear that printing additional layers improves the electrochemical response. Consequently, all the electrodes used next were made with three carbon coatings and cured at 90 °C for 45 minutes.

Amperometric detection of glucose in a lateral flow device

To demonstrate the suitability of these electrodes as electrochemical detectors in paper-based electroanalytical applications, we used the chips presented above to study the response of a glucose biosensor under flow conditions. Fusion 5 lateral flow membranes were mounted on devices featuring glucose biosensors (see Experimental section) as shown in Fig. 1. We chose Fusion 5 because it offers high wicking rates and can simultaneously fulfil the functions of the sample pad, strip, and wicking pad. Although a full description of the mass transport conditions inside the lateral flow membrane is beyond the scope of the present work, as in other hydrodynamic systems, steady-state currents showing a linear dependence on the concentration of the analyte were observed at a bare electrode (see Fig. 4S and 5S, ESI†).

To calibrate the biosensors, glucose solutions were allowed to flow through a Fusion 5 paper strip under fully wetted flow conditions.[34,35] This was achieved by placing a large wicking pad on the wide end of the strip. The working electrode was kept at 0.2 V *vs.* the upstream Ag/AgCl pseudo-reference electrode, which ensured oxidation of TMPD, and the current was recorded. Buffered glucose aliquots of increasing concentration were added every 120 seconds. A stable response was obtained 30 seconds after each addition (see Fig. 6S, ESI† for a typical chronoamperogram), and Fig. 6 shows the Michaelis–Menten plot for our glucose biosensor.

Human capillary blood samples were collected from a healthy volunteer's thumb using safety lancets (Sarstedt 85.1016). 50 μL of sample were spiked with 150 μL of a 10 mM glucose standard solution to make a final volume of 200 μL in microeppendorf tubes. Samples were used immediately after collection. After calibrating the biosensors using glucose standards of concentration ranging between 0.5 and 10 mM, the

Table 2 Comparison of the physical and electrochemical properties of different working electrodes in a typical batch (n = 3)

	Thickness (μm)	RMS (μm)	Water contact angle (°)	Track resistance (Ω)	ΔE_p (mV)	k_s [29]
Carbon – 1 layer	55 ± 2	2.7 ± 0.1	126 ± 2	83 ± 10	172 ± 9	$5.6 \times 10^{-6} \pm 8 \times 10^{-7}$
Carbon – 2 layers	68 ± 3	2.7 ± 0.1	129 ± 3	60 ± 8	120 ± 6	$1.4 \times 10^{-5} \pm 2 \times 10^{-6}$
Carbon – 3 layers	85 ± 5	2.8 ± 0.2	113 ± 7	49 ± 6	96 ± 9	$2.7 \times 10^{-5} \pm 4 \times 10^{-6}$
Ag/AgCl – 1 layer	55 ± 2	1.6 ± 0.1	109 ± 2			

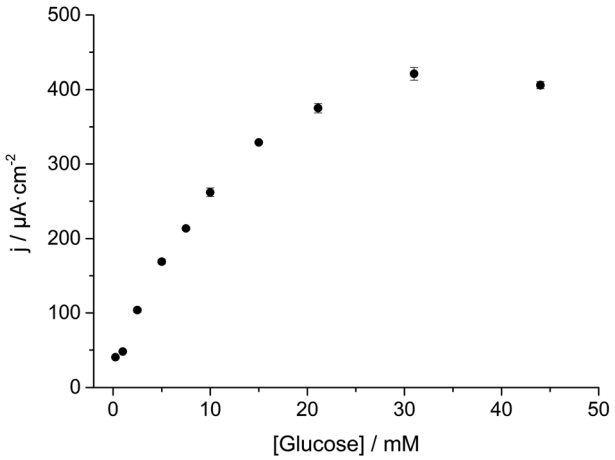

Fig. 6 Amperometric response to glucose solutions. Measurements were performed at 0.2 V *vs.* Ag/AgCl pseudo-reference electrode.

system was rinsed with 50 μL of buffer solution before approximately 50 μL of the test solution was run through the strip. Another drop of blood was analysed simultaneously using a commercial glucose meter (CardioCheck, Novalab, ES). A blood glucose concentration of 3.04 ± 0.3 mM (54.7 mg dL^{-1}) was determined using the commercial biosensor. A direct interpolation of the current measured by our biosensor using its calibration curve yielded a blood glucose concentration of 2.7 ± 1.2 mM (49 mg dL^{-1}). This low value compared to the commercial device is thought to be due to the higher viscosity of the blood sample compared to the glucose standards used. After flowing blood samples, the strips were rinsed with buffer and a new glucose standard aliquot was passed through the system. In this case the current measured was lower than before processing the blood sample. Blood cells present in the sample were retained in the membrane, so the lower current found was likely due to a combination of a lower flow rate and electrode passivation (see Fig. 6S, ESI†). Thus, although further work is required to improve the measurement reliability in blood, the loss of performance after a single use does not pose a significant problem for a disposable device.

Conclusions

We have presented a simple and versatile technique for the prototyping of electrodes using screen-printing pastes. Different electrode geometries and arrangements may be tested easily and modified according to experimental needs in a very short time and, since no screen or printing equipment is needed, the cost of changing the design is also very low.

The technique involves the fabrication of stencils by pre-cutting the protective liner of a pressure-sensitive adhesive tape. This pre-cutting may be carried out by different means, and in this work we have compared the results obtained from using a laser engraver and a cutter-plotter. Good results can be obtained by both approaches, although blade cutting provides superior performance when features as small as 250 μm are involved. Laser cutting, on the other hand, offers significantly faster processing speeds, and as a result is the preferred option when large structures (>2 mm) are involved. We strongly believe that this technique is ideal for prototyping purposes not only because of the small size of the structures that may be produced with a relatively low level of resources, but also because of the wide variety of materials that can be stencilled. Although we have used commercial graphite pastes, those based on other carbon forms or on other electroactive materials may be used, thus extending the applicability of the technique much further.

In addition, we have also demonstrated the successful combination of this rapid prototyping technique and lateral flow membranes to facilitate the development of electroanalytical devices, exemplified with the case of a glucose biosensor. Lateral flow membranes provide stable and reproducible hydrodynamic conditions in the absence of pumps, as well as working with small sample volumes similar to those used in conventional microfluidic applications. This makes it very easy to carry out sample or electrode treatment operations and to work with solutions of different composition using very small volumes.

Our results show that the approach presented here can be used to develop lateral flow tests with electrochemical detection easily and without the need for sophisticated screen-printing equipment.[36–38] Although the same technique could be applied for making adhesive stencils and transfer tapes,[17,39] the presence of an adhesive layer facilitates the integration of lateral flow membranes in the devices. In fact, the pressure sensitive adhesive used in this work is customarily used as a backing material in conventional lateral flow applications.

The introduction of electrochemical detection in lateral flow devices represents a more cost-effective approach to quantification than present optical systems based on fluorescence or colorimetry.[40] However, the main advantage of the presented approach is that, in line with rapid prototyping methods, it can reduce the development time and cost of new electrochemical devices and applications based on lateral flow.

Acknowledgements

This work has been funded by the Spanish Ministry of Economy through the DADDi2 project (Grant TEC2013-48506). MK acknowledges funding through the Beatriu de Pinós program (BP-DGR-2013), supported by the Secretary for Universities and Research of the Ministry of Economy and Knowledge of the Government of Catalonia and the Cofund programme of the Marie Curie Actions of the 7th R&D Framework Programme of the European Union.

Notes and references

1 C. Daniel and J. Hughes, *Microelectron. Reliab.*, 1968, 7, 137–143.

2 D. Erath, A. Filipović, M. Retzlaff, A. K. Goetz, F. Clement, D. Biro and R. Preu, *Sol. Energy Mater. Sol. Cells*, 2010, **94**, 57–61.
3 N. Nakayama, H. Matsumoto, A. Nakano, S. Ikegami, H. Uda and T. Yamashita, *Jpn. J. Appl. Phys.*, 1980, **19**, 703–712.
4 A. P. F. Turner, *Sens. Actuators*, 1989, **17**, 433–450.
5 M. A. Alonso-Lomillo, O. Dominguez-Renedo and M. J. Arcos-Martinez, *Talanta*, 2010, **82**, 1629–1636.
6 J. P. Metters, R. O. Kadara and C. E. Banks, *Analyst*, 2011, **136**, 1067–1076.
7 S. G. Stalnecker, *Electrocomponent Sci. Technol.*, 1980, **7**, 47–53.
8 K. Suganuma, *Introduction to printed electronics*, Springer, 2014.
9 N. Sani, M. Robertsson, P. Cooper, X. Wang, M. Svensson, P. A. Ersman, P. Norberg, M. Nilsson, D. Nilsson, X. J. Liu, H. Hesselbom, L. Akesso, M. Fahlman, X. Crispin, I. Engquist, M. Berggren and G. Gustafsson, *Proc. Natl. Acad. Sci. U. S. A.*, 2014, **111**, 11943–11948.
10 A. Määttänen, U. Vanamo, P. Ihalainen, P. Pulkkinen, H. Tenhu, J. Bobacka and J. Peltonen, *Sens. Actuators, B*, 2013, **177**, 153–162.
11 J. D. Newman and A. P. F. Turner, *Anal. Chim. Acta*, 1992, **262**, 13–17.
12 D. A. Bartholomeusz, R. W. Boutté and J. D. Andrade, *J. Microelectromech. Syst.*, 2005, **14**, 1364–1374.
13 D. Snakenborg, H. Klank and J. P. Kutter, *J. Micromech. Microeng.*, 2004, **14**, 182–189.
14 M. J. Gonzalez-Guerrero, J. P. Esquivel, D. Sanchez-Molas, P. Godignon, F. X. Munoz, F. J. del Campo, F. Giroud, S. D. Minteer and N. Sabate, *Lab Chip*, 2013, **13**, 2972–2979.
15 J. Moral-Vico, J. Barallat, L. Abad, R. Olive-Monllau, F. X. Munoz-Pascual, A. G. Ortega, F. J. del Campo and E. Baldrich, *Biosens. Bioelectron.*, 2015, **69**, 328–336.
16 L. Renaud, D. Selloum and S. Tingry, *Microfluid. Nanofluid.*, 2015, **18**, 1407–1416.
17 N. Godino, R. Gorkin 3rd, K. Bourke and J. Ducree, *Lab Chip*, 2012, **12**, 3281–3284.
18 S. Byrnes, G. Thiessen and E. Fu, *Bioanalysis*, 2013, **5**, 2821–2836.
19 C. L. Cassano and Z. H. Fan, *Microfluid. Nanofluid.*, 2013, **15**, 173–181.
20 D. Zang, L. Ge, M. Yan, X. Song and J. Yu, *Chem. Commun.*, 2012, **48**, 4683–4685.
21 S. J. Vella, P. Beattie, R. Cademartiri, A. Laromaine, A. W. Martinez, S. T. Phillips, K. A. Mirica and G. M. Whitesides, *Anal. Chem.*, 2012, **84**, 2883–2891.
22 W. J. Lan, E. J. Maxwell, C. Parolo, D. K. Bwambok, A. B. Subramaniam and G. M. Whitesides, *Lab Chip*, 2013, **13**, 4103–4108.
23 A. W. Martinez, S. T. Phillips, G. M. Whitesides and E. Carrilho, *Anal. Chem.*, 2010, **82**, 3–10.
24 A. W. Martinez, S. T. Phillips, E. Carrilho, S. W. Thomas, H. Sindi and G. M. Whitesides, *Anal. Chem.*, 2008, **80**, 3699–3707.
25 M. R. Deakin, K. J. Stutts and R. M. Wightman, *J. Electroanal. Chem.*, 1985, **182**, 113–122.
26 G. Cui, J. H. Yoo, J. S. Lee, J. Yoo, J. H. Uhm, G. S. Cha and H. Nam, *Analyst*, 2001, **126**, 1399–1403.
27 M. Islam, R. Natu and R. Martinez-Duarte, *Microfluid. Nanofluid.*, 2015, **19**, 973–985.
28 A. Toossi, M. Daneshmand and D. Sameoto, *J. Micromech. Microeng.*, 2013, **23**, 9.
29 I. Lavagnini, R. Antiochia and F. Magno, *Electroanalysis*, 2004, **16**, 505–506.
30 R. G. Compton and C. E. Banks, *Understanding Voltammetry*, Imperial College Press, 2nd edn, 2010.
31 T. J. Davies, R. R. Moore, C. E. Banks and R. G. Compton, *J. Electroanal. Chem.*, 2004, **574**, 123–152.
32 E. P. Randviir, D. A. C. Brownson, J. P. Metters, R. O. Kadara and C. E. Banks, *Phys. Chem. Chem. Phys.*, 2014, **16**, 4598.
33 K. Grennan, A. J. Killard and M. R. Smyth, *Electroanalysis*, 2005, **17**, 1360–1369.
34 E. L. Fu, S. Ramsey, P. Kauffman, B. Lutz and P. Yager, *Microfluid. Nanofluid.*, 2011, **10**, 29–35.
35 J. L. Osborn, B. Lutz, E. Fu, P. Kauffman, D. Y. Stevens and P. Yager, *Lab Chip*, 2010, **10**, 2659–2665.
36 K. Abe, K. Kotera, K. Suzuki and D. Citterio, *Anal. Bioanal. Chem.*, 2010, **398**, 885–893.
37 A. Murphy, B. Gorey, K. de Guzman, N. Kelly, E. P. Nesterenko and A. Morrin, *RSC Adv.*, 2015, **5**, 93162–93169.
38 M. Medina-Sanchez, M. Cadevall, J. Ros and A. Merkoçi, *Anal. Bioanal. Chem.*, 2015, **407**, 8445–8449.
39 A. S. Afonso, C. V. Uliana, D. H. Martucci and R. C. Faria, *Talanta*, 2016, **146**, 381–387.
40 E. W. Nery and L. T. Kubota, *Anal. Bioanal. Chem.*, 2013, **405**, 7573–7595.